

Evaluating commercial marine emissions and their role in air quality policy using observations and the CMAQ model



Allison M. Ring^{a,*}, Timothy P. Canty^a, Daniel C. Anderson^{a,1}, Timothy P. Vinciguerra^b, Hao He^a, Daniel L. Goldberg^c, Sheryl H. Ehrman^b, Russell R. Dickerson^{a,d,e}, Ross J. Salawitch^{a,d,e}

^a Department of Atmospheric and Oceanic Science, University of Maryland, College Park, MD 20742, USA

^b Department of Chemical and Biomolecular Engineering, University of Maryland, College Park, MD 20742, USA

^c Energy Systems Division, Argonne National Laboratory, Argonne, IL 60439, USA

^d Earth System Science Interdisciplinary Center, University of Maryland, College Park, MD 20742, USA

^e Department of Chemistry and Biochemistry, University of Maryland, College Park, MD 20742, USA

ARTICLE INFO

Keywords:

Surface ozone
OMI satellite
Commercial marine vessel
Air quality
Emissions inventory
Community Multiscale Air Quality (CMAQ) model

ABSTRACT

We investigate the representation of emissions from the largest (Class 3) commercial marine vessels (c3 Marine) within the Community Multiscale Air Quality (CMAQ) model. In present emissions inventories developed by the United States Environmental Protection Agency (EPA), c3 Marine emissions are divided into off-shore and near-shore files. Off-shore c3 Marine emissions are vertically distributed within the atmospheric column, reflecting stack-height and plume rise. Near-shore c3 Marine emissions, located close to the US shoreline, are erroneously assumed to occur only at the surface. We adjust the near-shore c3 Marine emissions inventory by vertically distributing these emissions to be consistent with the off-shore c3 Marine inventory. Additionally, we remove near-shore c3 Marine emissions that overlap with off-shore c3 Marine emissions within the EPA files.

The CMAQ model generally overestimates surface ozone (O_3) compared to Air Quality System (AQS) site observations, with the largest discrepancies occurring near coastal waterways. We compare modeled O_3 from two CMAQ simulations for June, July, and August (JJA) 2011 to surface O_3 observations from AQS sites to examine the efficacy of the c3 Marine emissions improvements. Model results at AQS sites show average maximum 8-hr surface O_3 decreases up to ~ 6.5 ppb along the Chesapeake Bay, and increases ~ 3 – 4 ppb around Long Island Sound, when the adjusted c3 Marine emissions are used.

Along with the c3 Marine emissions adjustments, we reduce on-road mobile NO_x emissions by 50%, motivated by work from Anderson et al. 2014, and reduce the lifetime of the alkyl nitrate species group from ~ 10 days to ~ 1 day based on work by Canty et al. 2015, to develop the “c3 Science” model scenario. Simulations with these adjustments further improve model representation of the atmosphere. We calculate the ratio of column formaldehyde (HCHO) and tropospheric column nitrogen dioxide (NO_2) using observations from the Ozone Monitoring Instrument and CMAQ model output to investigate the photochemical O_3 production regime (VOC or NO_x -limited) of the observed and modeled atmosphere. Compared to the baseline, the c3 Science model scenario more closely simulates the HCHO/ NO_2 ratio calculated from OMI data.

Model simulations for JJA 2018 using the c3 Science scenario show a reduction of surface O_3 by as much as ~ 13 ppb for areas around the Chesapeake Bay and ~ 2 – 3 ppb at locations in NY and CT downwind of New York City. These reductions are larger in 2018 than in 2011 due to a change in the photochemical O_3 production regime in the Long Island Sound region and the projected decline of other (non-c3 Marine) sources of O_3 precursors, highlighting the importance of proper representation of c3 Marine emissions in future modeling scenarios.

1. Introduction

Tropospheric ozone (O_3) is a harmful secondary pollutant regulated

by the United States Environmental Protection Agency (EPA). The Clean Air Act (CAA) passed in 1970, and subsequent amendments, have led to continued reductions of atmospheric pollutants and improved air

* Corresponding author.

E-mail address: aring1@umd.edu (A.M. Ring).

¹ Now at: Department of Chemistry, Drexel University, Philadelphia, PA 19104, USA.

quality across the US [EPA, 1970; 1990]. One mandate of the CAA required establishment of the National Ambient Air Quality Standards (NAAQS), which provides states with clear attainment requirements for six “criteria pollutants” harmful to public health. States with areas designated as non-attainment, meaning concentrations of regulated pollutants are above the federal standard, are required to submit a State Implementation Plan (SIP) to the EPA. These plans outline how state environmental agencies, through regulatory efforts, policy enforcement, and proposed emissions limitations from upwind sources, intend to meet the required attainment standard. SIPs rely on data and modeling simulations to support proposed regulatory strategies [Cohan and Chen, 2014; Digar et al., 2011].

Nitrogen dioxide (NO₂) and O₃ are criteria pollutants, with attainment standards of 100 ppb 1-hr average [EPA, 2010] and 70 ppb 8-hr average, respectively [EPA, 2015c]. These compounds have long been a primary focus of state and federal agencies when developing air quality attainment strategies for the SIP process. Based on the most recent national emissions inventory, the largest contributor to the total anthropogenic NO_x (NO + NO₂) budget in the US is the transportation sector (~56%) which includes on-road vehicles, off-road vehicles, aircraft, commercial marine vessels, and locomotives. Electrical generating units contribute ~25% to the total NO_x budget and consist of commercial fuel combustion, industrial boilers, and residential heating. Industrial processes like cement and chemical manufacturing, mining, oil and gas production, etc. account for ~11% of anthropogenic NO_x, and the remainder comes from biomass burning, gas stations and waste disposal activities (~8%) [EPA, 2016]. Due to the anthropogenic contribution, air quality attainment strategies usually focus on the largest NO_x emitters like electrical generating units (EGUs) and mobile (on-road and off-road) sources.

Many studies have shown elevated pollution levels around waterways [Cooper, 2003; Goldberg et al., 2014; Lawrence and Crutzen, 1999; Murphy et al., 2009; Pirjola et al., 2014; Williams et al., 2009], an important consideration for states with coastlines. Higher levels of criteria pollutants are observed at Air Quality System (AQS) monitoring sites near the coasts along heavily trafficked marine waterways [Gégo et al., 2007; Mazzuca et al., 2016; Stauffer et al., 2015; Yu et al., 2006]. It is estimated that approximately 80% of goods traded globally are transported via commercial marine vessels (CMVs) [Pirjola et al., 2014], and that emissions from CMVs contribute approximately 15–30% to the global anthropogenic NO_x budget [Corbett et al., 2007; Eyring et al., 2005; Williams et al., 2009]. Due to the immense number and international identity of CMVs, NO_x regulation and enforcement are difficult, even when ships are operating in near-shore shipping lanes and port environments [Eyring et al., 2005; Pirjola et al., 2014].

To manage emissions from CMVs, the International Maritime Organization (IMO) has instituted controls for diesel engine vessels in specified Emission Control Areas (ECA); zones that extend 200 nautical miles off the coast of participating countries [EPA, 2008]. The US petitioned the IMO to include the North American continent in the International Convention for the Prevention of Pollution from Ships (MARPOL) Annex VI, an international agreement that regulates air pollution from large ocean-going vessels, allowing the US and Canada to regulate CMV emissions within ECAs [EPA, 2008; 2009b]. The US was successfully added to the list of IMO participating countries in 2008, requiring all class 3 commercial marine vessels (c3 Marine) operating within US coastal waters to comply with IMO regulations [EPA, 2008]. As of 2015, ~50% of the c3 Marine global fleet is 20+ years old, ~20% is between 10 and 20 years, and ~30% is less than 10 years old [UN, 2015]. This means ships younger than 20 years old (~50% of the global fleet) are required to meet the Tier I IMO emissions regulations (17 g/kWh of NO_x at idle) passed in 2000 [IMO, 2014]. As more of the global fleet is retired, new vessels must meet the more stringent global Tier II regulations (14.4 g/kWh of NO_x at idle) and Tier III regulations (3.4 g/kWh of NO_x at idle) if operating within ECAs [IMO, 2014].

The main engines of most commercial marine vessels are run solely for propulsion while auxiliary engines are run continuously to meet all other energy demands for ship operation. NO_x emissions rates from these two engine types are highly dependent upon fuel composition and engine temperatures. The slower the ships are moving, the longer and hotter these engines are running, resulting in higher NO_x emissions [Cooper, 2003]. Commercial marine vessels are also a significant source of large particles called giant cloud condensation nuclei (GCCN), contributing to enhanced boundary layer cloud formation [Sorooshian et al., 2015] as well as particulate matter with a diameter < 2.5 μm (PM_{2.5}), a criteria pollutant that contributes to hundreds of thousands of premature deaths globally [Cohan and Chen, 2014; Cohen et al., 2005; Corbett and Koehler, 2003; Pope et al., 2002].

Elevated levels of tropospheric O₃ over CMV traveled bodies of water have been measured by both *in situ* and remote techniques [Cleary et al., 2015; Goldberg et al., 2014]. Advection of this polluted air over coastal land and cities may contribute to the elevated pollution over these regions [Loughner et al., 2011; Loughner et al., 2014; Stauffer et al., 2015] and at coastal AQS monitoring sites. For major metropolitan cities near heavily trafficked CMV areas like Baltimore, MD, Philadelphia, PA, and New York, NY, the development of attainment strategies addressing CMV emissions will become increasingly important as global shipping activity is projected to increase in the future [EPA, 2009b; McDill et al., 2015].

In this paper, we investigate the role of CMV emissions on regional air quality, and the representation of this pollution source within a regulatory air quality model. We adjust the vertical distribution of emissions from the largest (class 3) commercial marine vessels, and examine the effect of this adjustment on surface O₃ production for various model simulations conducted for years 2011 and 2018. Comparisons of modeled surface O₃ to AQS data, and modeled column formaldehyde (HCHO) and NO₂ to satellite measurements, are used to evaluate model performance for 2011. We also quantify the effect of an improved model framework for a 2018 SIP attainment strategy developed by the Maryland Department of the Environment (MDE).

2. Model description

2.1. The CMAQ platform

We use the Community Multiscale Air Quality (CMAQ) model version 5.0.2 [Byun and Schere, 2006], an EPA approved regulatory air quality model used by state and federal agencies to develop surface O₃ attainment strategies. CMAQ v5.0.2 uses the 2005 Carbon Bond (CB05) chemical mechanism consisting of 156 chemical reactions with 51 species representing the photochemistry of the troposphere [Yarwood et al., 2005]. An updated version of CB05 called the Carbon Bond Mechanism version 6 (CB6) was released in 2010 [Yarwood et al., 2010], however it is not publically available for use with CMAQ at the time of paper submission. All CMAQ simulations have 12 km × 12 km horizontal resolution, with the model domain covering the eastern half of the United States.

Meteorological input was generated by the EPA using the Weather Research Forecasting (WRF) version 3.4 model [Skamarock et al., 2008] for the year 2011 and processed with Meteorological Chemistry Interface Processor (MCIP) version 4.2 [Otte and Pleim, 2010] to reformat WRF output for use in CMAQ [EPA, 2014]. For biogenic emissions, we use the Biogenic Emission Inventory System (BEIS) version 3.61, which incorporates improved vegetation data, land use cover data, and canopy model formulation [Bash et al., 2016].

All anthropogenic emissions used for this study are the Alpha 2 version, developed by the Mid Atlantic Regional Air Management Association (MARAMA) [McDill et al., 2015] and based on the EPA 2011 National Emissions Inventory (2011 NEI) version 2 data [EPA, 2015a]. Emissions inventories for year 2018 are generated by applying growth factors for all inventory sectors to the 2011 base case emissions

[McDill et al., 2015].

Various sector emissions are gridded to CMAQ resolution and merged into daily 3-D, temporally varying input files using the Sparse Matrix Operator Kernel Emissions (SMOKE) version 3.6 [CMAS, 2014]. Model output from CMAQ is generated for June 1st through August 31st for 2011 and 2018, the three hottest and most important months for photochemical O₃ production during the O₃ season (April–October). We compare CMAQ output from the 2011 base case simulation to observations for the same period. The 2018 CMAQ output is used to examine the effectiveness of future emissions reductions and proposed policies.

2.2. Commercial marine vessel emissions inventory

This study focuses on the class 3 commercial marine vessel inventory, which represents emissions for marine diesel engines with fuel displacement of 30 L/cylinder or larger [EPA, 2002; 2009b; 2015a]. This emissions sector mainly consists of cruise ships and international open ocean vessels, used in transporting consumer goods and resources.

The EPA generated the total c3 Marine emissions values for the 2011 NEI by applying growth factors to ship emissions data acquired in 2002 [EPA, 2002; 2009b]. These growth factors account for a variety of policies and changes in shipping activity that affect the 2011 inventory year, including the ECA regulations described above and global NO_x and sulfur dioxide (SO₂) controls [EPA, 2015a; McDill et al., 2015]. The spatial distribution of CMV emissions are generated using data from the Research and Innovative Technology Administration's Bureau of Transportation Statistics National Transportation Atlas Database, the US Census Bureau, GIS shapefiles provided by ports, and satellite imagery such as Google Earth. [EPA, 2009a; ERG, 2010]. This method was refined for the 2014 NEI, improving county designation and grid point locations within state waters [EPA, 2015b]. Similar studies have used data from the Automatic Identification System (AIS), which provides detailed information about ship location, speed, ship activities, navigational plans, and many other parameters [Chen et al., 2016; Chen et al., 2017a, 2017b]. Due to the large data volume, computational intensity, complexity and scale of US coastal operations, AIS was not used to develop 2011 or 2014 CMV emissions, however it is recommended for future inventory development [EPA, 2015b; Eyth and Driver (EPA), 2017].

For the c3 Marine sector, the emissions inventory is divided between off-shore and near-shore emissions. The EPA is responsible for the development of off-shore c3 Marine emissions, designated as outside state waters and within the IMO established ECA. Conversely, near-shore emissions are designated to be within state waters close to coastlines, and thus the EPA requests that states gather and report this information [EPA, 2015a]. If near-shore emissions from states are incomplete, the EPA emissions are used.

Fig. 1 shows the spatial extent of near-shore (a) and off-shore (b) emissions within our CMAQ modeling domain. The off-shore emissions are designated as point sources, allowing for the vertical distribution of emissions above the surface, reflecting the stack heights of the ships, along with plume rise and dispersion of the emissions. Near-shore c3 Marine emissions are designated as area sources, so all emissions are assumed to occur only in the surface layer of the model. This different designation results in inconsistent modeling of c3 Marine emissions and erroneously places high levels of NO_x and other c3 Marine emissions from the near-shore files at the surface of heavily trafficked waterways like the Chesapeake and Delaware Bays, New York Harbor, and Long Island Sound. It also prevents CMAQ from accurately simulating vertical mixing and transport of these emissions.

3. Data description

3.1. Satellite data

The Ozone Monitoring Instrument (OMI) is a joint atmospheric monitoring project among three countries. The instrument was developed by a team of scientists from the Netherlands and Finland and is deployed aboard the NASA Aura satellite, which orbits with a suite of other satellites in the NASA A-train. Aura was launched in 2004 and has a polar, sun synchronous orbit providing daily global coverage with an overpass time of approximately 13:45 local solar time (LST) at the equator [Levelt et al., 2006a; Levelt et al., 2006b]. The OMI instrument measures solar radiation backscattered from the atmosphere and Earth's surface within the UV/Visible wavelength range of 270–500 nm, with a spatial resolution of 13 km × 24 km at nadir and total swath coverage of 2600 km. The OMI science team retrieves column O₃, NO₂, and SO₂, three of the six criteria pollutants named by the EPA, as well as column BrO, OCIO, and HCHO [Levelt et al., 2006a; Levelt et al., 2006b]. A detector row anomaly appeared in the data on June 25, 2007 and impacted approximately 50% of OMI pixels in 2011, significantly reducing data density [Bucseles et al., 2013]. All pixels affected by the row anomaly in the OMI products described below are filtered out of our analysis [Boersma et al., 2011; Bucseles et al., 2013].

We focus on two OMI data products: daily tropospheric column NO₂ and column HCHO. We use these products to examine the ability of CMAQ to accurately represent the chemistry that controls photochemical O₃ production [Duncan et al., 2010]. For NO₂, we use the NASA Goddard Space Flight Center (GSFC) version 3 level 2 tropospheric column product retrieval [Bucseles et al., 2013; Krotkov and Veefkind, 2016; Krotkov et al., 2017] gridded to 0.25° latitude × 0.25° longitude resolution. For HCHO, we use version 3 level 2 reference sector corrected swath product from the Harvard-Smithsonian Astrophysical Observatory (SAO) retrieval [González Abad et al., 2015] also on a 0.25° latitude × 0.25° longitude grid. For both OMI products, we only use pixels that satisfy quality and row anomaly flags, have a cloud fraction less than 30%, and a solar zenith angle less than 70°. Additionally, data from the two outer most pixels are removed due to their large footprint (28 km × 150 km) compared to the nadir view. Both retrievals are publically available at <http://mirador.gsfc.nasa.gov>.

Since HCHO concentrations in the stratosphere are negligible [Millet et al., 2006], the HCHO retrieval does not incorporate a stratosphere-troposphere separation algorithm. Instead, *a priori* HCHO profiles are generated using GEOS-Chem simulations. These vertical profiles are used to develop the air mass factor (AMF) calculations at various latitudes. This profile extends up to 100 hPa where the concentrations of HCHO have dropped to near 0 ppb [González Abad et al., 2015]. Total column NO₂ has a non-negligible stratospheric contribution, therefore, a stratosphere-troposphere separation algorithm based on Global Modeling Initiative (GMI) output is used to isolate the stratospheric and tropospheric components of the total column observations [Bucseles et al., 2013; Krotkov et al., 2017]. We use tropospheric NO₂ and total column HCHO data for June, July and August 2011 to compare with CMAQ output.

3.2. Air Quality System data

The Air Quality System (AQS) is an EPA and Office of Air Quality Planning and Standards network of more than 4,000 surface monitoring stations throughout the US that measure ambient air pollution. The principal goal of the network is to examine the exposure of the US population to a variety of pollutants. AQS data are available from 1980 to the present for approximately 500 species, must pass several quality control checks before distribution, and are publicly available at <https://www.epa.gov/outdoor-air-quality-data> [EPA, 2016]. In this study, we compare maximum 8-hr O₃ data collected at AQS sites to model output within our modeling domain. We use model output to compute design

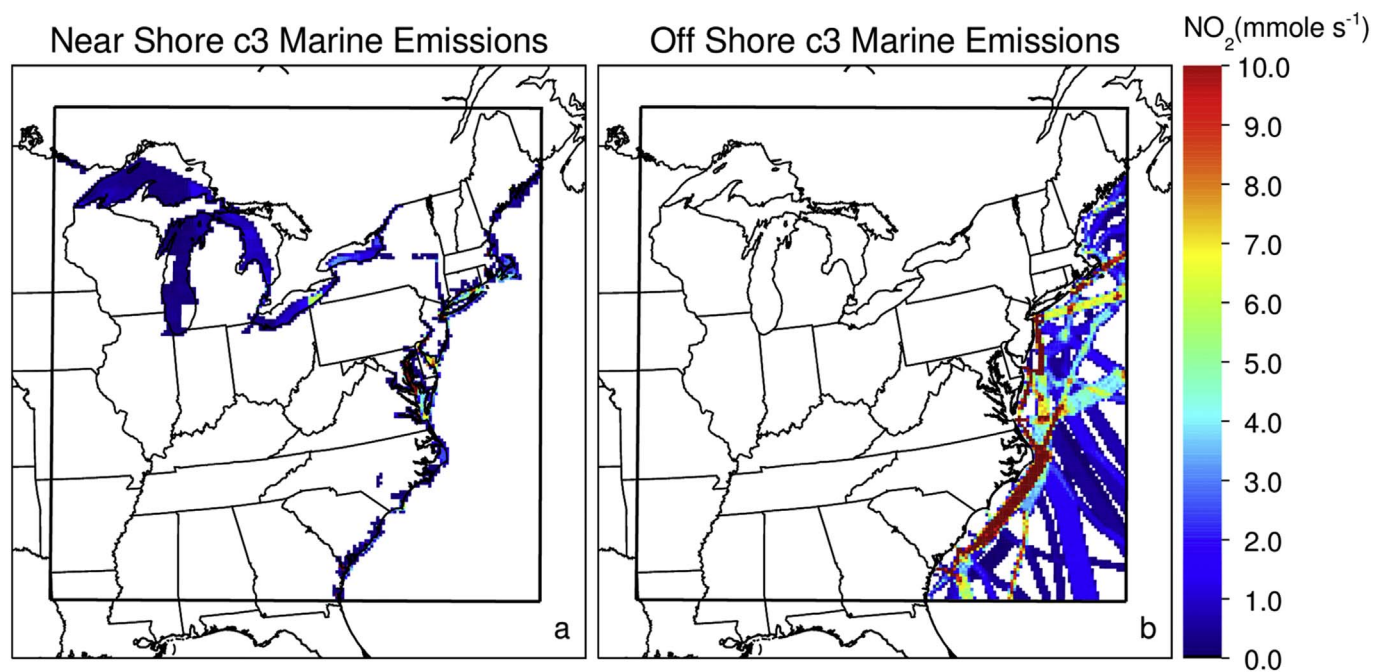


Fig. 1. Average class 3 commercial marine vessel (c3 Marine) NO_2 inventory emissions at 2pm LST for June, July, and August 2011 are shown for (a) near-shore and (b) off-shore emissions files. Black boxes in (a) and (b) outline the CMAQ model domain.

values, and compare these to data based calculated design values at each AQS site [EPA, 2015a]. Design Values (DVs) are a metric used to determine NAAQS areas of attainment and areas of non-attainment, an important distinction influencing local and regional science policy [Wayland, 2014].

4. Class 3 marine vessel emissions adjustment

As discussed in section 2.2, near-shore c3 Marine emissions occur within the surface layer of the model while off-shore c3 Marine emissions are vertically distributed in model layers above the surface. We attempt to rectify this discrepancy by using an appropriate average profile calculated based on nearby, off-shore c3 Marine emissions, and apply this profile to the near-shore c3 Marine emissions.

Fig. 2a shows the near-shore c3 Marine emissions are divided into seven regions. Regional division is necessary because the off-shore c3

Marine emissions are regionally dependent throughout the model domain. Therefore, an average vertical profile for the whole domain would not accurately represent geographic and temporal variability. Implementing adjustment regions for the near-shore c3 Marine emissions roughly preserves these variations. The seven regions were chosen based on coastal separations already present within the files (Fig. 2a).

While determining the adjustment regions, overlapping points between the near-shore and off-shore c3 Marine emissions files were discovered. An example is shown in Fig. 2b for the MD/VA region, with overlapping points marked by a smaller blue circle.

There should be no overlap between the near-shore and off-shore files, an issue likely created from trying to reconcile and combine state and EPA generated c3 Marine emissions. To correct this oversight, we set the near-shore emissions to zero for these overlapping points, and retained the off-shore emissions values. This adjustment corrected the over counting, and preserved the vertical distribution of c3 Marine

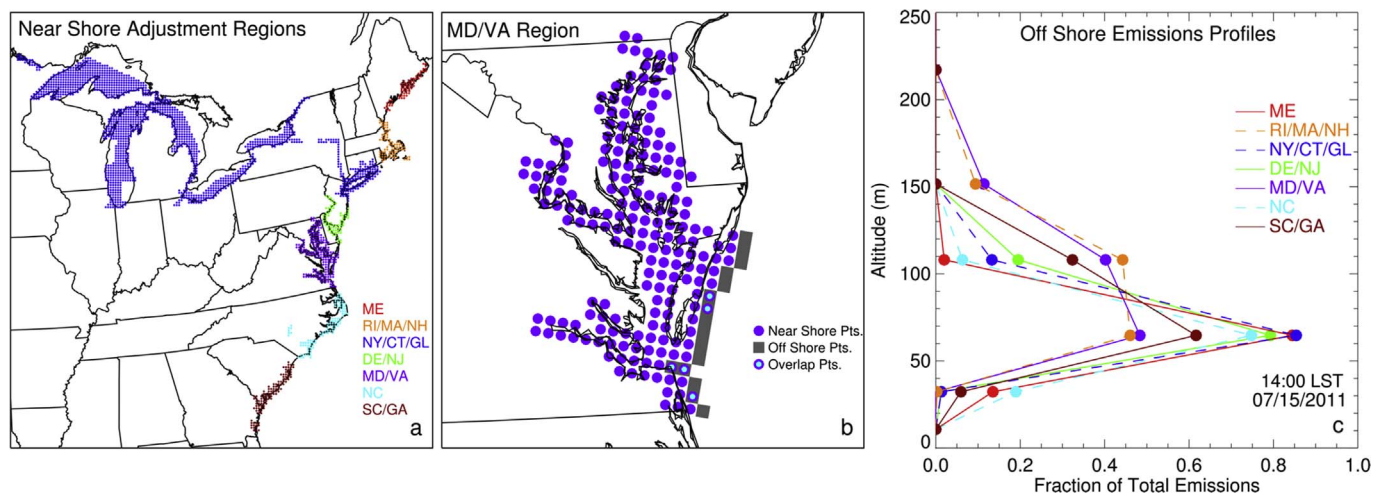


Fig. 2. (a) Near-shore c3 Marine emissions geographically divided into 7 adjustment regions. All near-shore c3 Marine emissions grid points are color coded to show regional designation. (b) The MD/VA region near-shore c3 Marine emissions grid points (purple filled circles), off-shore emissions grid points (gray squares), and overlapping grid points (purple and blue circles). (c) Average vertical fractional distribution of off-shore c3 Marine emissions for each region at 14:00 LST on July 15, 2011 plotted at the half-height of the emissions layer.

emissions for these grid points.

Off-shore emissions grid points bordering the near-shore adjustment regions were used to calculate the average vertical distribution profile for each region. An example is shown in Fig. 2b. The gray boxes represent the grid points with off-shore c3 Marine emissions used to calculate the average vertical distribution profile for the near-shore MD/VA adjustment region. This profile was then used to vertically distribute the near-shore emissions within the adjustment region at the grid points represented by the purple circles in Fig. 2b. The c3 Marine emissions vary hourly, so the average profile was calculated for each hour of each day and applied to the appropriate near-shore region. As an example, average vertical distribution profiles calculated for each adjustment region at 14:00 EST on July 15, 2011 are shown in Fig. 2c. Finally, the adjusted near-shore c3 Marine emissions were removed from the daily area source near-shore file and added to the corresponding daily point source off-shore file to create a single c3 Marine emissions inventory file. This ensured all c3 Marine emissions data were modeled consistently within CMAQ, as point source emissions.

5. Results and discussion

5.1. 2011 modeling and data comparison

Various modeling simulations for June, July, and August (JJA) 2011 and 2018 were conducted. In addition to baseline model simulations, we perform model runs that incorporate observationally driven adjustments to the on-road mobile emissions inventory [Anderson et al., 2014; Travis et al., 2016] and modifications to the CB05 chemical mechanism [Canty et al., 2015]. Combinations of these two changes, along with the c3 Marine adjustment, comprise the various modeling scenarios discussed in this paper.

The first adjustment addresses on-road mobile NO_x emissions throughout the modeling domain. Analysis of aircraft observations indicate emissions from this sector are high by a factor of two in the EPA inventory [Anderson et al., 2014; Travis et al., 2016]. Consequently, we apply a 50% reduction to mobile NO_x emissions throughout the domain. The second adjustment corrects the expectation that the alkyl-nitrate radical group (NTR) in CB05, has a lifetime of ~10 days for loss by photolysis. This is much longer than the actual photolytic lifetime of most of the chemical species comprising the NTR group, so we reduce the lifetime by a factor of 10 to a more realistic ~1 day lifetime [Canty et al., 2015]. It is important to note that CB05 assumes 100% recycling of NO_x, which contributes to increased O₃ production within the model relative to a more realistic treatment of NO_x [Canty et al., 2015]. The final adjustment is the change to the vertical distribution of c3 Marine emissions explained in section 4. Table 1 details the various model and emissions inventory adjustments made for each modeling scenario discussed in this paper.

We use average maximum 8-hr O₃ (AM8O₃) as a metric to analyze model output and compare with ground based observations. We follow the EPA guidelines for calculating maximum daily average 8-hr O₃ (MDA8) [EPA, 2015c], which are summarized as follows. A forward running 8-hr mean (MDA8) is calculated for each day at each grid cell within the model. The maximum MDA8 within a 3 × 3 grid is then

attributed to the center grid cell. For the JJA time frame, we average the MDA8 for the top 10 days above 60 ppb at each grid cell. This is known as the AM8O₃ value. To calculate AM8O₃ for corresponding simulations of future air quality, in this case 2018, the MDA8 assigned to the center grid cell of the 3 × 3 grid in 2018 is co-located with the MDA8 cell used in the 3 × 3 grid in 2011.

The geographic area for this analysis is narrowed from the full model domain to a region encompassing the coastal Mid-Atlantic and Northeast states that highlights locations with large, highly active commercial ports near heavily populated areas and some of the highest levels of observed surface O₃. This study region is outlined in subsequent figures by a black dashed line.

Fig. 3a shows AM8O₃ for the baseline model simulation. As shown in Table 1, the 2011 Baseline simulation does not include any model adjustments. The 2011 c3 Adjust scenario (Fig. 3b) incorporates the near-shore c3 Marine vertical distribution adjustments, described in section 4. The difference between these two simulations (Fig. 3c) reveals the areas within our study domain that show considerable changes in surface AM8O₃ due to the improved vertical representation of c3 Marine emissions. The decrease in surface AM8O₃ over the Chesapeake Bay and closely surrounding areas is due to the c3 Marine adjustment moving O₃ precursor emissions off the surface, and distributing them vertically within the atmosphere. This modification allows some emissions to be vented out of the boundary layer, improving model representation of atmospheric pollution transport, resulting in a significant (~6 ppb) decline of surface AM8O₃ over the Chesapeake Bay. The increase of surface AM8O₃ shown in the New York and Connecticut regions is due to increased pollution transport from upwind c3 Marine sources, and the non-linear chemistry that controls O₃ production, discussed later in section 5.2.

Comparisons of surface model O₃ output to surface O₃ data from AQS locations are shown for the 2011 Baseline (Fig. 3d) and 2011 c3 Adjust (Fig. 3e) modeling scenarios. Within our study region, we compare AQS AM8O₃ calculated from observations to modeled AM8O₃ from the CMAQ grid point closest to the AQS site. Comparison of Fig. 3d and e shows the effect of the c3 Marine emissions vertical distribution adjustment. Modeled AM8O₃ at some AQS locations increases, while at others it decreases, however, almost all the modeled AM8O₃ is too high compared to observations. For instance, the AQS site at Greenwich Point Park, CT has a measured AM8O₃ value of ~80 ppb and a modeled AM8O₃ value of ~150 ppb for both scenarios. A high bias in CMAQ model of surface AM8O₃ has been shown in prior studies and is an area of active research [Canty et al., 2015; Loughner et al., 2014; Trail et al., 2014; Travis et al., 2016; Vinciguerra et al., 2017]. The comparisons shown in Fig. 3d and e highlight the limitations of CMAQ to accurately model surface O₃ on specific days, under certain meteorological conditions, particularly for coastal regions.

Fig. 3f shows the change in modeled surface AM8O₃ at each AQS location when the vertical distribution of c3 Marine emissions is improved. Model values at AQS sites with differences less than 0.05 ppb are not included. We find the largest increases of modeled AM8O₃ at some AQS sites in New York and Connecticut, discussed in the next section, and we see the largest decreases at some AQS sites in Maryland. At the AQS site in Furley, MD, the model shows an AM8O₃ decrease of

Table 1

Description of the four CMAQ modeling scenarios and their appropriate inventory and model adjustments.

Modeling scenario	c3 Marine emissions adjustment	On-Road mobile emissions inventory adjustment	Alkyl nitrate radical (NTR) lifetime adjustment
Baseline	No adjustment	No adjustment	No adjustment
c3 Adjust Science	Adjusted emissions (see section 4)	No adjustment	No adjustment
	No adjustment	Adjusted emissions decrease NO _x by 50% (Anderson et al., 2014; Travis et al., 2016)	Reduced NTR lifetime from 10 days to 1 day (Canty et al., 2015)
c3 Science	Adjusted emissions (see section 4)	Adjusted emissions decrease NO _x by 50% (Anderson et al., 2014; Travis et al., 2016)	Reduced NTR lifetime from 10 days to 1 day (Canty et al., 2015)

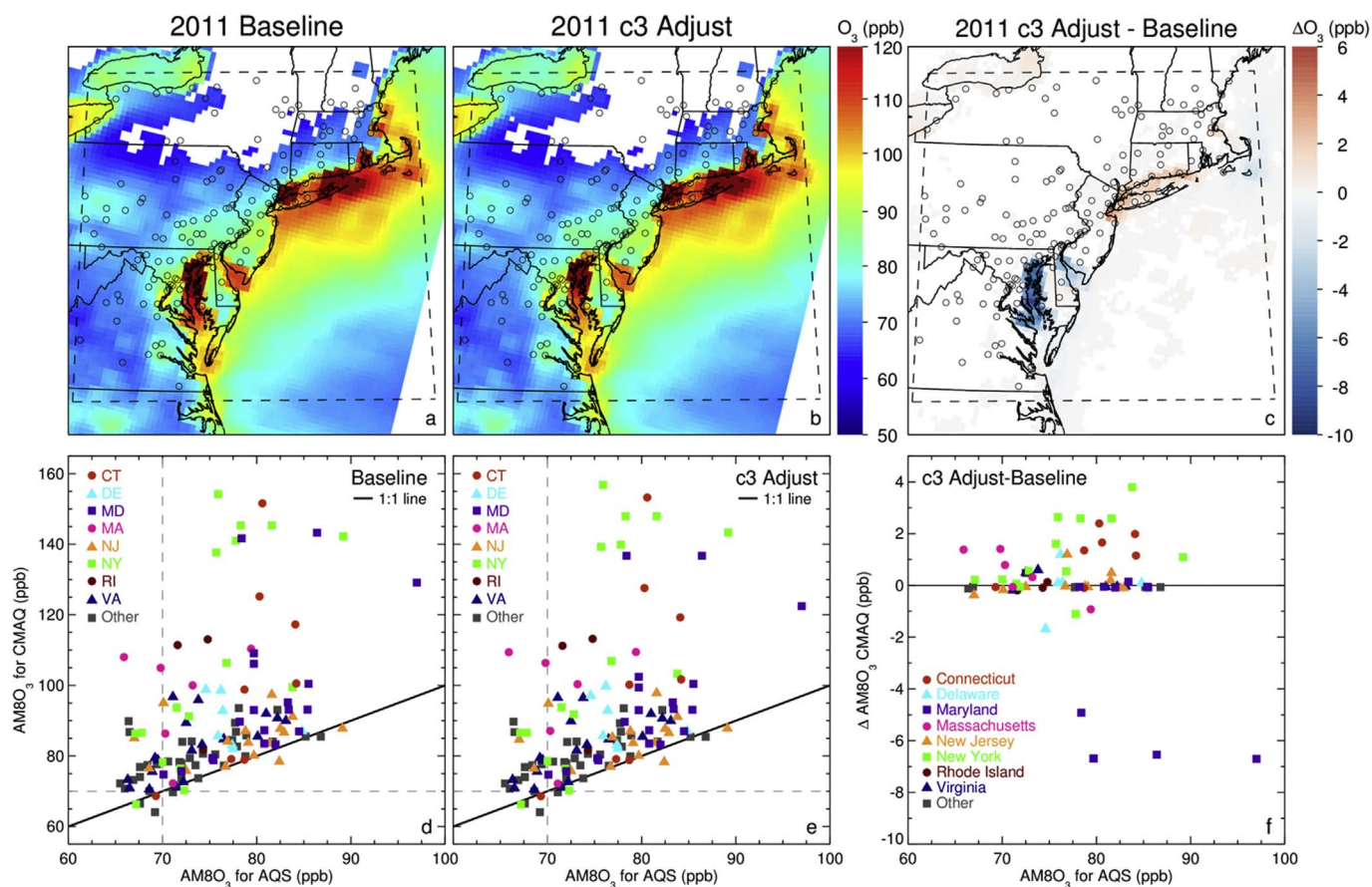


Fig. 3. Average maximum 8-hr ozone ($AM8O_3$) for June, July, and August 2011 for (a) Baseline and (b) c3 Adjust model scenarios. If the $AM8O_3$ criteria are not met, model output is not shown (white regions within domain). Black dashed lines in upper plots outline the focus region for this study. Open black circles represent AQS O_3 monitoring station locations. (c) The $AM8O_3$ difference between Baseline and c3 Adjust. (d) A scatter plot of $AM8O_3$ for Baseline vs AQS data, with points color coded by state. (e) A scatter plot of $AM8O_3$ for c3 Adjust vs AQS data. (f) The change in $AM8O_3$ between the c3 Adjust and Baseline model scenarios at AQS locations.

~4.9 ppb, while the Edgewood, MD, Essex, MD, Calvert, MD, Blackwater NWR, MD sites show decreases of over 6 ppb. All five AQS sites border the Chesapeake Bay, with Essex, Edgewood, and Furley all located near Baltimore, MD. This reduction of modeled $AM8O_3$ in Maryland is of considerable magnitude, an important result for state and federal agencies developing air quality policy.

5.2. Evaluation of CMAQ output with satellite retrievals

The photochemical production of O_3 is non-linearly dependent upon ambient NO_x and volatile organic compound (VOC) concentrations [Jacob, 2000; Kleinman et al., 2001; Kleinman, 2005; Sillman, 1999, 2002]. This dependence leads to an optimal VOC: NO_x ratio that produces the maximum amount of tropospheric O_3 and represents the transition region between two atmospheric states: one where O_3 production is limited by the concentration of VOCs (VOC-limited) and the other where O_3 production is NO_x -limited. Understanding the state of the actual atmosphere, along with how O_3 production is represented within regulatory air quality models, is crucial for developing attainment strategies that will properly inform air quality policy decisions.

If the local atmosphere is NO_x -limited, reducing NO_x emissions will have the desired policy effect of decreasing tropospheric O_3 concentrations. In a locally VOC-limited environment, reducing NO_x will have the undesired effect of increasing local concentrations of tropospheric O_3 , until the reductions of NO_x are large enough to place O_3 production in the NO_x limited regime. Presently, VOC-limited conditions are present in megacities and major metropolitan areas such as New York, NY, Houston, TX, and Los Angeles, CA [Duncan et al., 2010; Kleinman, 1994; Kleinman et al., 2000; Madronich, 2014; Mazzuca

et al., 2016], making air quality control especially challenging for these areas. In a VOC-limited environment, reductions in both VOCs and NO_x are typically necessary to improve surface O_3 . Previous studies have shown that the Baltimore-Washington area has successfully transitioned to a NO_x -limited regime [Duncan et al., 2010; Goldberg et al., 2016; He et al., 2013; Liao et al., 2014]. The CMAQ simulations presented in Fig. 3 indicate NO_x -limited conditions for the Baltimore-Washington region because reductions of surface NO_x emissions, due to the adjustment of the vertical profile of c3 Marine emissions, lead to a decrease in modeled surface O_3 (Fig. 3c and f). Conversely, the surface O_3 increases shown in the New York City, Connecticut, and Long Island Sound region in Fig. 3c are indicative of a region where O_3 production is VOC-limited, at least within the model.

Further analysis into the photochemical regime for O_3 production in the New York metropolitan area is performed using OMI satellite observations of column HCHO and NO_2 . Daily retrievals of HCHO and NO_2 on a 0.25° latitude \times 0.25° longitude grid were used to calculate average HCHO and NO_2 for JJA 2011. We first calculate the standard deviations (σ) of the HCHO and NO_2 data at each grid point. We require there to be at least 10 coincident days of data for both HCHO and NO_2 at each grid point, that fall within two standard deviations (2σ). Finally, we calculate the average HCHO and NO_2 values at each grid point over the period.

For comparison to CMAQ, we apply the averaging kernel (AK) from the retrievals to the model output for HCHO and NO_2 . The AKs were calculated by dividing the Air Mass Factor (AMF) for HCHO and the tropospheric AMF for NO_2 by the scattering weight reported for each retrieval, as described in Gonzalez Abad et al. [2015]. Model output from 14:00 LST, was log-linearly interpolated to the satellite pressure

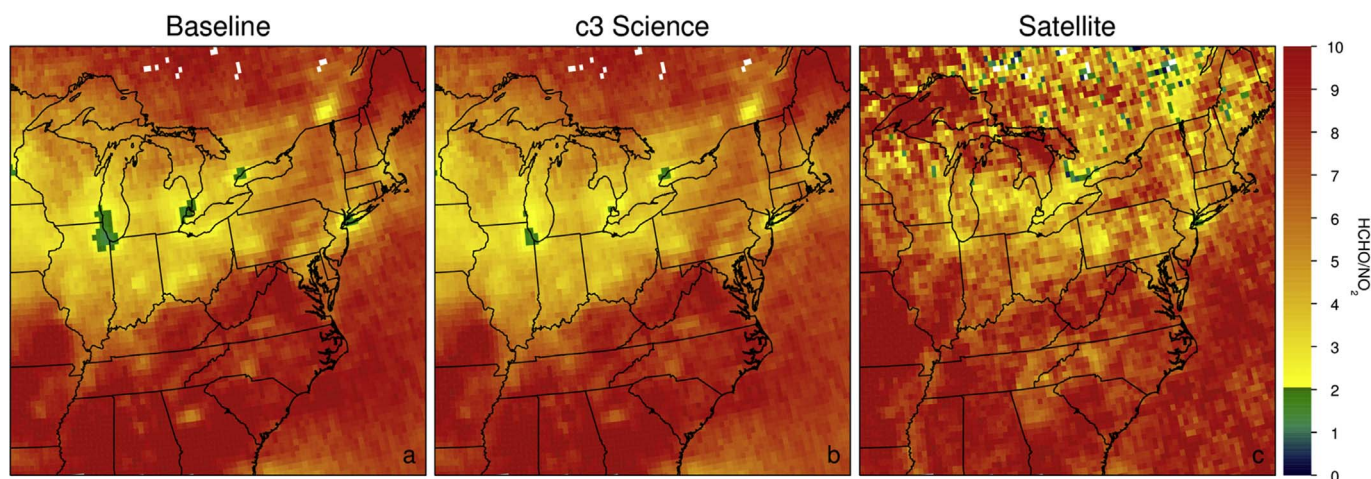


Fig. 4. Ratio of average column HCHO to average tropospheric column NO_2 for (a) Baseline scenario, (b) c3 Science scenario, (c) OMI satellite data, over the model domain for JJA 2011. Only grid points with at least 10 days of satellite data for both HCHO and NO_2 retrievals are used. Model output for the two scenarios are convolved with appropriate OMI SAO (HCHO retrieval) and OMI GSFC (NO_2 retrieval) averaging kernels.

level at each model grid point, and then multiplied by the corresponding AK from the closest overlapping satellite pixel. The resulting product was then integrated to calculate a column value for both HCHO and NO_2 , comparable to the satellite column observations. These CMAQ-based columns were then averaged onto the same 0.25° latitude \times 0.25° longitude grid at the satellite data, based on the criteria used to calculate the average satellite HCHO and NO_2 values, detailed above. This method ensures consistency between the satellite data and model output used in the analysis.

Fig. 4 shows the average column HCHO/average tropospheric column NO_2 ratio (hereafter, HCHO/ NO_2 ratio) from CMAQ output and satellite data for the modeling domain. According to Duncan et al. [2010], a HCHO/ NO_2 ratio between 1 and 2 indicates the atmospheric column is transitioning between VOC-limited and NO_x -limited regimes. When the ratio is below 1, the atmosphere is considered to be VOC-limited, and when the ratio is above 2, the atmosphere is considered to be NO_x -limited. Fig. 5 is the same as Fig. 4, except it focuses on the New York metropolitan region. Fig. 5a shows that for the baseline CMAQ model scenario, the air above New York City (NYC) and Eastern Long Island has a HCHO/ NO_2 ratio between 1 and 2 (green boxes), indicating that the atmosphere is transitioning between the VOC and NO_x -limited regimes [Duncan et al., 2010]. In Fig. 5b, the c3 Science model scenario (detailed in Table 1) shows the area downwind of NYC is mostly transitioned to a NO_x -limited atmosphere (yellow and orange boxes), leaving a smaller area over NYC within the transition zone. Fig. 5c shows the average satellite HCHO/ NO_2 ratio, indicating that some areas over NYC are within the transition zone while most of the area is within the NO_x -limited regime. Fig. 5b shows too much of the NYC region as transitioned to NO_x -limited conditions, compared to the satellite ratio (Fig. 5c). This is likely due to the 50% reduction of mobile NO_x emissions in the c3 Science model scenario. This reduction was applied domain wide, based on an empirical study that was completed for the Baltimore-Washington region [Anderson et al., 2014]. While the 50% reduction in mobile NO_x is a good approximation of the necessary emissions inventory adjustment, further modeling studies should adjust the mobile NO_x emissions inventory on a more localized scale, based on observational data throughout the model domain.

Fig. 5d and e are scatter plots of the Baseline CMAQ HCHO/ NO_2 ratio to the satellite HCHO/ NO_2 ratio, and the c3 Science model HCHO/ NO_2 ratio to the satellite HCHO/ NO_2 ratio, respectively. Linear least squares fits to the data points, forced to go through the origin (0-intercept) are also shown. These comparisons indicate that the c3 Science scenario is more closely representative of the observed atmosphere, as evidenced by the 0-intercept slope of 0.97 compared to the 0-intercept

slope of 0.92 for the Baseline scenario. In Fig. 5d and e, points below the 1 to 1 line indicate the model is producing a lower HCHO/ NO_2 ratio than expected. This could mean there is too little HCHO, or too much NO_2 in the model column compared to the satellite retrieval. When the c3 Science model framework is used (Fig. 5e), the number of points below the 1 to 1 line are reduced, especially for ratio values < 5 . Since the model improvements mostly affect column NO_x concentrations, this suggests that the adjustments are improving the representation of NO_x within the model. Additionally, for the Chesapeake Bay region, both the Baseline and c3 Science model frameworks are representative of observed satellite HCHO/ NO_2 ratios (Figure SF1), accurately representing the area as completely NO_x -limited.

For some regions of the model domain, like the upper mid-west, both model simulations produce HCHO/ NO_2 ratios that are lower than observed (see Fig. 4). In more rural regions, we see no improvement in the HCHO/ NO_2 ratio between the two model scenarios, which could suggest the low ratios are due to HCHO. This is likely due to the CB05 chemical mechanism used by CMAQ. When the improved chemical mechanism CB6r2 is used [Ruiz and Yarwood, 2013], HCHO concentrations increase within the model, and are more consistent with measured values [Goldberg et al., 2016]. Further improvements to the CB6r2 chemical mechanism, will increase HCHO concentrations within the model [Marvin et al., 2017], and should improve model performance when compared to satellite observations. In the Chicago and Detroit metropolitan centers, we see increases in the HCHO/ NO_2 ratio when model improvements are applied (Figures SF2 and SF3, respectively). This is expected as decreases of NO_x in urban centers would raise the HCHO/ NO_2 ratio.

Based on satellite comparison, the c3 Science scenario more accurately represents the state of the 2011 atmosphere. While further improvements to HCHO and NO_x representation in rural regions within the model are necessary, the c3 Science scenario improves the representation of O_3 photochemistry in urban centers throughout the modeling domain, creating a more realistic model framework for guiding public policy.

5.3. 2018 modeling scenarios

To assist state agencies in developing air quality attainment strategies, future emissions estimates are generated based on expected economic growth factors, fleet turnover, future air quality regulations, etc. Development of the future emissions inventory aids in providing guidance and justification for emissions standards reductions and proposed government legislation to improve air quality. We use the 2018

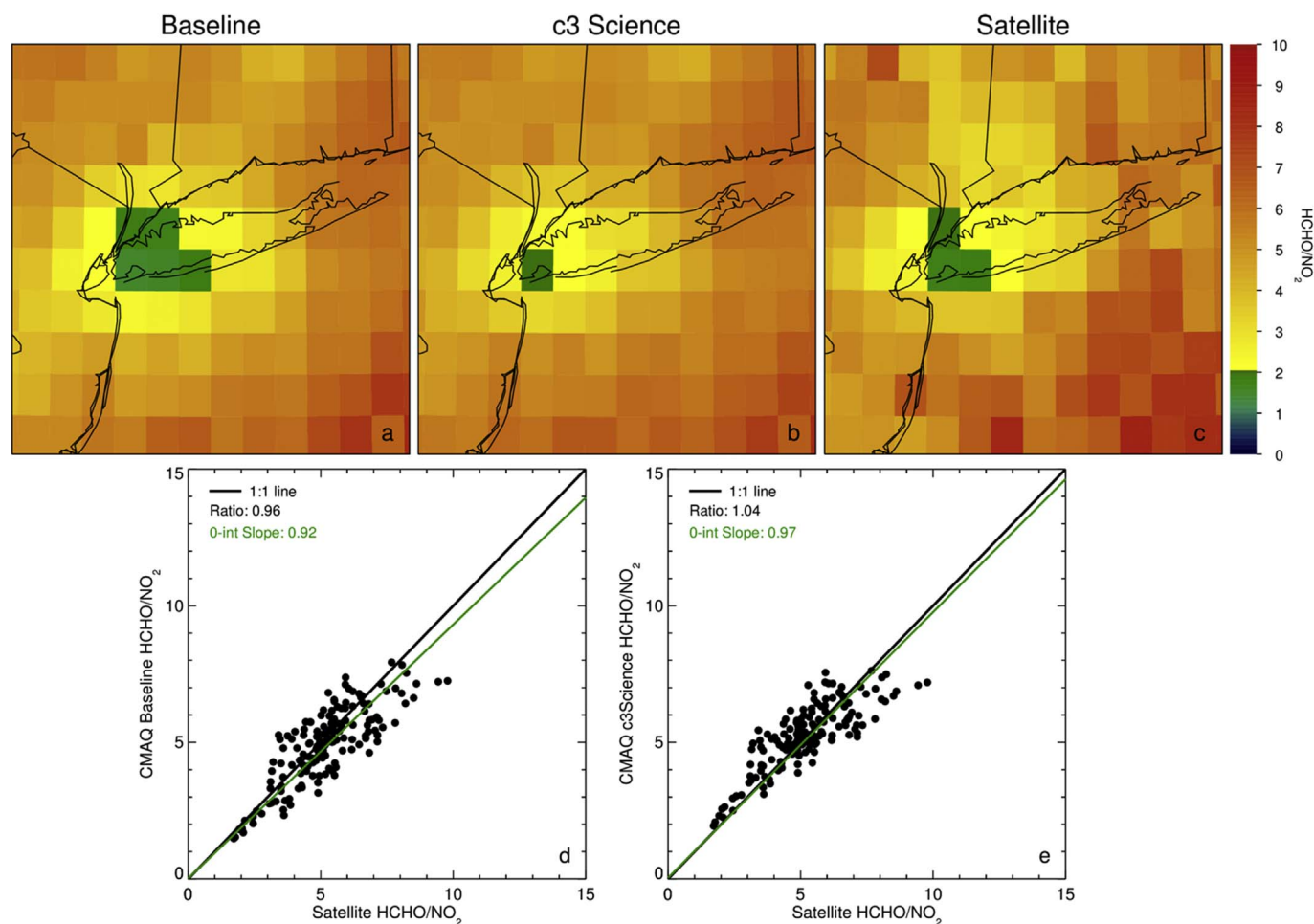


Fig. 5. The top row is the same as Fig. 4, except focusing on the NY metropolitan region. Scatter plots comparing the satellite derived HCHO/NO₂ ratio and the (d) Baseline scenario ratio, and (e) c3 Science scenario ratio are shown.

projected emissions to examine the efficacy of the c3 Science model scenario in 2018 compared to 2011, and to assess a future attainment strategy developed by MDE, discussed in section 5.4.

All 2018 model scenarios discussed in this section use the same meteorology as the 2011 simulations, therefore, all differences in O₃ between 2011 and 2018 are due solely to emissions. AM8O₃ for the 2018 Baseline simulation is shown in Fig. 6a. Modeled surface O₃ in 2018 is notably lower than in 2011 (Fig. 3a), indicative of the expected air quality improvements that will occur by 2018. Values of AM8O₃ for the 2018 c3 Science simulation are shown in Fig. 6b. Fewer model grid points are plotted for the c3 Science scenario than in the Baseline scenario, because some grid points no longer satisfy the criteria of 10 days with maximum 8-hr O₃ above 60 ppb in the 2011 simulation. Elevated O₃ levels are still present in the Chesapeake Bay and Long Island Sound; however, these regions are smaller and have a reduced magnitude when compared to 2011.

A scatter plot of AM8O₃ at the CMAQ grid points closest to the AQS monitoring sites for the Baseline and c3 Science model scenarios is shown in Fig. 6c. Some grid points in NJ, CT, and NY for example, are above the 1 to 1 line, indicating surface AM8O₃ increases in the c3 Science model scenario relative to the Baseline simulation. Conversely, all points in MD, and some in NY, as well as CT lie below the 1 to 1 line, indicating a reduction of AM8O₃ in the c3 Science scenario relative to the Baseline scenario. Sites with the highest AM8O₃ shown in Fig. 6c are listed in Table 2. Values in the last column are bolded for sites showing reductions of AM8O₃ between the two model scenarios.

When comparing AM8O₃ for Baseline and c3 Science scenarios, it is important to remember there are three major modeling framework

changes that comprise the c3 Science scenario, as described in Table 1. Decreasing the lifetime of NTR contributes to the domain wide increase (red color) shown in Fig. 6d. Since 2018 emissions are scaled based on 2011 emissions, the 50% reduction of on-road mobile NO_x emissions in 2018 is also necessary. This reduction is less effective in 2018 because the on-road mobile emissions are projected to be cleaner due to national regulations, fleet turnover, new fuel requirements, and local control programs despite a projected increase in vehicle miles traveled [McDill et al., 2015]. Essentially, further controls of on-road mobile emissions will be less effective because this NO_x source sector has already been significantly reduced. Large reductions of surface O₃ within the Chesapeake Bay and increases in the coastal NY metropolitan area are shown in Fig. 6d. These are due to the c3 Marine emissions inventory adjustments, described in section 4.

As noted earlier, CMAQ produces extremely high values of modeled AM8O₃ (> 140 ppb) for some locations (Fig. 6c). These high values are much larger than measured surface O₃ in 2011 and are therefore unrealistic. Nevertheless, model results at the six AQS sites with the highest AM8O₃ in 2018 show greater reductions of surface O₃ in the c3 Science scenario. This demonstrates the worst days for modeled surface O₃ in 2018 are more improved in the c3 Science model scenario when compared to the Baseline scenario.

We now return to the impact of c3 Marine emissions on NO_x and VOC limits of the photochemical O₃ production. AM8O₃ decreases of ~5–15 ppb are shown in Fig. 6d for grid points in the Chesapeake Bay region. Conversely, increases of ~2–6 ppb are shown for grid points in New York/New Jersey Harbor and Long Island Sound. We see regions of AM8O₃ decrease downwind of New York City, a different result from

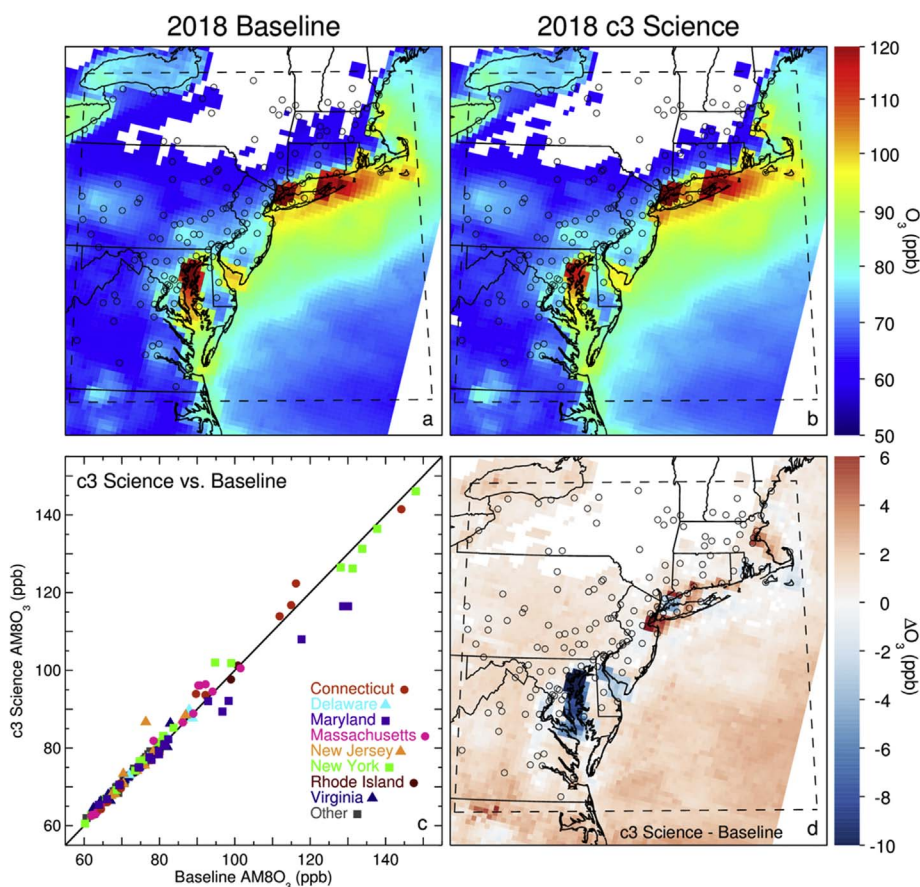


Fig. 6. AM8O₃ for JJA 2018 for (a) Baseline and (b) c3 Science model scenarios. (c) A scatter plot of AM8O₃ for model grid points closest to the AQS sites for the Baseline vs. c3 Science scenarios. (d) A difference plot between c3 Science and Baseline model scenarios, highlighting AM8O₃ changes in the Chesapeake Bay and along the NYC metropolitan area coast.

Table 2
AQS sites with highest modeled AM8O₃ shown in Fig. 6c.

AQS site	2018 baseline (AM8O ₃ PPB)	2018 c3 science (AM8O ₃ PPB)	ΔAM8O ₃ (PPB)
Pfizer Lab, NY	148.0	146.0	-2.0
Greenwich Point, CT	144.2	141.4	-2.8
Queens College, NY	137.8	136.4	-1.4
White Plains, NY	133.8	131.3	-2.5
Babylon, NY	131.3	126.2	-5.1
Riverhead, NY	128.1	126.5	-1.6
Essex, MD	130.1	116.5	-13.6
Furley, MD	128.8	116.5	-12.3
Sherwood Island, CT	116.2	122.3	6.1
New Haven, CT	114.9	116.8	1.9
Fort Griswold Park, CT	111.9	113.9	2.0
Edgewood, MD	117.7	108.0	-9.7

2011 (Fig. 3c). To further emphasize this point, Fig. 7 highlights the impact of ship emissions on surface O₃ production along coastal regions within the 2011 and 2018 Science model framework (Table 1). In both Fig. 7a and b we see the expected decreases in AM8O₃ within the Chesapeake and Delaware Bay regions. In 2018 (Fig. 7b), the AM8O₃ reductions are larger, showing more dramatic effects on surface O₃ production when large precursor sources (c3 Marine emissions) are lifted off the surface. Additionally, Fig. 7a and b shows smaller increases in AM8O₃ in the NJ/NY/CT area in 2018 than in 2011. Comparing Fig. 7a and b highlights the reduction of AM8O₃ in the New York metropolitan area and along the Connecticut coast in 2018, perhaps showing parts of the region are transitioned and others have yet to transition from a VOC to NO_x-limited region for photochemical O₃ production within the model.

5.4. Air quality attainment strategy analysis

State agencies use air quality models to quantify the effect of proposed legislation on future air quality. Here we examine one attainment strategy developed by MDE called “Scenario 4A”. This approach assumes that in 2018, emissions from EGUs will be at the best observed rates between 2005 and 2012 using existing emissions control equipment. To examine the impact of this attainment strategy on reducing surface O₃ production, Fig. 8 shows the effect of implementing scenario 4A regulations within the c3 Science model framework. Implementing the Scenario 4A attainment strategy reduces AM8O₃ domain wide, with the largest reductions occurring in areas significantly affected by power plants.

To quantify the AM8O₃ reduction in 2018 due to various scenario changes, we use Design Values (DV) as required by the EPA. An observed yearly design value is the 3-year running average of the observed fourth highest daily peak 8-hr average O₃ at an AQS site. The base design value (DVB) is a weighted average of yearly design values over a 5-year period [Wayland, 2014]. The second column of Table 3 provides 2011 DVs for select AQS monitoring sites.

To assess attainment strategies for future years, a surface O₃ relative response factor (RRF) is calculated. This metric represents the fractional change in modeled surface O₃ based on emissions changes between the base and future modeling scenarios [Wayland, 2014]. For this analysis, the RRF is the AM8O₃ for 2018 divided by the AM8O₃ for 2011. The design value for the future model scenario (DVF) is the RRF multiplied by the DVB at each evaluated monitoring site. This value is compared to the NAAQS standards to determine whether the location of the monitoring site, in the simulated attainment strategy, is in attainment [Wayland, 2014].

We have calculated DVs for four modeling scenarios. The scenarios are:

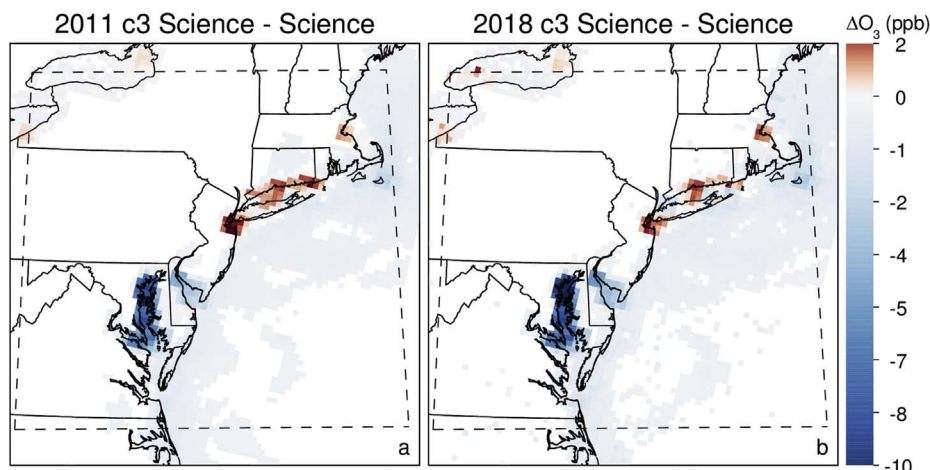


Fig. 7. Difference plots of AM8O₃ between the c3 Science and Science modeling scenarios for (a) 2011 and (b) 2018. This highlights the effect of the c3Marine adjustment on surface O₃ production in the Science model framework.

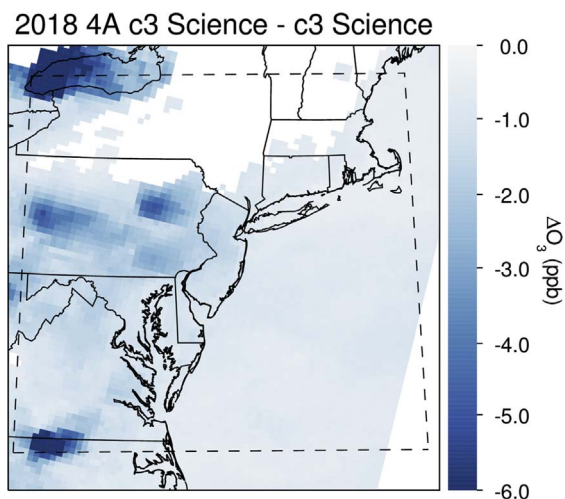


Fig. 8. The difference of modeled AM8O₃ between c3 Science simulations both with and without the Scenario 4A attainment strategy adjustments.

1. 2011 Baseline to 2018 Baseline
2. 2011 Baseline to 2018 Baseline with Scenario 4A emissions reductions
3. 2011 c3 Science to 2018 c3 Science
4. 2011 c3 Science to 2018 c3 Science with Scenario 4A emissions reductions

The DVs at selected AQS sites are shown in columns 3–6 of Table 3. Results shown in Table 3 indicate the effectiveness of the Scenario 4A power plant emissions reductions in both the baseline and c3 Science model scenarios (columns 7 and 8). As expected, all DVs are negative in the two columns, meaning the 4A scenario is effective at reducing surface O₃ at all monitoring sites. Focusing on the italicized values in Table 3 columns 7 and 8 that denote the larger of the two differences for each site, we see Scenario 4A emissions reductions are more effective at reducing surface O₃ in the c3 Science model scenario than in the Baseline scenario for almost all AQS locations; an important, policy relevant finding.

6. Conclusions

In this study, we examine the impact of Class 3 Commercial Marine

Table 3

Observed and modeled design values calculated for several modeling scenarios at AQS sites in CT/NY/MD. Bolded values in last two columns show largest ΔDVF.

Air quality attainment strategy (Scenario 4A) analysis							
AQS site	DVB	DVF Baseline	DVF 4A Baseline	DVF c3 Science	DVF 4A c3 Science	ΔDVF 4A Base - Base	ΔDVF 4A c3 Science - c3 Science
Greenwich Point, CT	80.3	76.37	76.12	71.54	71.15	-0.25	-0.39
Stratford Point, CT	84.3	77.30	76.76	76.53	75.98	-0.54	-0.55
Sherwood Island, CT	83.7	82.95	82.51	78.88	78.43	-0.44	-0.45
Hammonasset, CT	85.7	75.69	75.32	76.25	75.88	-0.37	-0.37
Pfizer Lab, NY	74.0	71.02	70.63	66.36	65.93	-0.39	-0.43
Queens College, NY	78.0	73.93	73.44	69.97	69.56	-0.49	-0.41
Babylon, NY	83.3	76.86	76.59	73.15	72.87	-0.27	-0.28
White Plains, NY	75.3	73.20	72.79	67.73	67.25	-0.41	-0.48
Davidsonville, MD	83.0	71.10	70.28	73.71	72.78	-0.82	-0.93
Padonia, MD	79.0	70.44	69.27	71.98	70.69	-1.17	-1.29
Essex, MD	80.7	73.24	72.85	72.24	71.73	-0.39	-0.51
Fair Hill, MD	83.0	73.78	72.64	75.97	74.62	-1.14	-1.35
Southern Maryland, MD	79.0	70.58	69.40	72.19	70.91	-1.18	-1.28
Fredrick Airport, MD	76.3	67.10	65.42	69.18	67.43	-1.68	-1.75
Edgewood, MD	90.0	82.02	81.47	82.41	81.67	-0.55	-0.74
Aldino, MD	79.3	70.14	69.41	72.22	71.34	-0.73	-0.88
Millington, MD	78.7	69.53	68.66	71.62	70.65	-0.87	-0.97
Rockville, MD	75.7	65.69	64.91	67.08	65.98	-0.78	-1.10
HU-Beltsville, MD	79.0	67.70	66.82	69.46	68.44	-0.88	-1.02
PG Equestrian Center, MD	82.3	70.52	69.64	72.85	71.84	-0.88	-1.01
Beltsville, MD	80.0	68.59	67.65	71.22	70.14	-0.94	-1.08

Vessels (c3 Marine) emissions on air quality of coastal regions along the eastern US. Class 3 vessels are the largest within the global shipping fleet, and have diesel engines with fuel displacement of at least 30 L/cylinder. We have adjusted near-shore c3 Marine emissions to reflect a more realistic and consistent vertical distribution of pollutants. Model results which include the adjusted c3 Marine emissions show a decrease of AM8O₃ at Maryland AQS sites near the Chesapeake Bay, such as Essex, MD: ~6.5 ppb, where photochemical O₃ production is NO_x-limited. In areas such as Long Island Sound, the vertical distribution adjustment of marine emissions has increased AM8O₃ by ~3.5 ppb. This result, driven by a reduction of NO_x near the surface within the model, is due to the primary local production of O₃ being within the VOC-limited regime. Additionally, elevation of near-shore c3 Marine emissions off the surface allows the model to more accurately represent pollution dispersion and transportation associated with the c3 Marine emissions. This increases the lifetime of these chemical species within the model because they are no longer remaining near the emission source, over-producing O₃ in most regions and/or being removed from the atmosphere via wet or dry deposition. Therefore, pollution transport from the Chesapeake Bay to the NY Metropolitan region could also contribute to increased surface O₃ production.

Column HCHO and NO₂ retrievals from the Ozone Monitoring Instrument (OMI) are used to calculate HCHO/NO₂ ratios to determine the O₃ production regime in the atmospheric column above the surface for observations and model simulations. In the Baseline CMAQ model scenario, the HCHO/NO₂ ratio shows a larger area over the New York metropolitan area is transitioning from VOC-limited to NO_x-limited than is observed from the satellite. When empirically based model improvements are incorporated, known as the c3 Science scenario (see Table 1), a greater area over the New York metropolitan is NO_x-limited, improving model performance in relation to the observed satellite HCHO/NO₂ ratio and more accurately representing tropospheric conditions.

We also examine the impact of these model improvements on future (2018) modeling scenarios. When comparing the 2018 Baseline to the c3 Science scenario, AM8O₃ reductions are larger for the Chesapeake Bay (Essex, MD: ~13.6 ppb), and smaller increases are shown for the New York metropolitan area than in 2011. Some regions around Long Island Sound show reductions in surface O₃, indicating the area has transitioned to NO_x-limited in the 2018 model simulation.

Analysis of a NAAQS attainment strategy developed by MDE that simulates EGUs operating with optimal emissions rates shows that the strategy is more effective within the c3 Science scenario. Simulations using this improved model framework predict greater decreases in surface O₃, indicating legislation aimed at limiting O₃ precursors should be more effective than is demonstrated by the Baseline CMAQ model simulation.

Finally, we note that previous studies have used satellite observations of tropospheric column NO₂ to develop top down commercial marine vessel emissions inventories [Lamsal et al., 2011; Vinken et al., 2014]. Presently, c3 Marine emissions inventories are generated by the EPA for subsequent years by applying growth factors to 2002 data. Constraining marine inventories to satellite observations, and using more detailed ship tracking data, such as the AIS, would improve the magnitude and spatial representation of the emissions for the modeling year. One challenge for the Eastern U.S. is distinguishing the signature of c3 Marine emissions in satellite observations from continental outflow that saturates the NO₂ retrieval. The use of satellite measurements to constrain marine emissions in the Eastern U.S. is the subject of current research being conducted by our group.

Acknowledgments

We greatly appreciate financial support for this work provided by the National Aeronautics and Space Administration (NASA) Atmospheric Composition Modeling and Analysis Program (ACMAP

#NNX15AE31G), the NASA Aura science team, and the Maryland Department of the Environment. We also appreciate the valuable guidance received via correspondence with Julie McDill from MARAMA, Alison Eyth and Laurel Driver from the EPA.

Appendix A. Supplementary data

Supplementary data related to this article can be found at <http://dx.doi.org/10.1016/j.atmosenv.2017.10.037>.

References

- Anderson, D.C., et al., 2014. Measured and modeled CO and NO_y in DISCOVER-AQ: an evaluation of emissions and chemistry over the eastern US. *Atmos. Environ.* 96, 78–87. <http://dx.doi.org/10.1016/j.atmosenv.2014.07.004>.
- Bash, J.O., Baker, K.R., Beaver, M.R., 2016. Evaluation of improved land use and canopy representation in BEIS v3.61 with biogenic VOC measurements in California. *Geosci. Model Dev.* 9 (6), 2191–2207. <http://dx.doi.org/10.5194/gmd-9-2191-2016>.
- Boersma, K.F., et al., 2011. An improved tropospheric NO₂ column retrieval algorithm for the ozone monitoring instrument. *Atmos. Meas. Tech.* 4 (9), 1905–1928. <http://dx.doi.org/10.5194/amt-4-1905-2011>.
- Bucselu, E.J., Krotkov, N.A., Celarier, E.A., Lamsal, L.N., Swartz, W.H., Bhartia, P.K., Boersma, K.F., Veefkind, J.P., Gleason, J.F., Pickering, K.E., 2013. A new stratospheric and tropospheric NO₂ retrieval algorithm for nadir-viewing satellite instruments: applications to OMI. *Atmos. Meas. Tech.* 6 (10), 2607–2626. <http://dx.doi.org/10.5194/amt-6-2607-2013>.
- Byun, D., Schere, K.L., 2006. Review of the governing equations, computational algorithms, and other components of the models-3 Community Multiscale Air Quality (CMAQ) modeling system. *Appl. Mech. Rev.* 59 (1–6), 51–77. <http://dx.doi.org/10.1115/1.2128636>.
- Canty, T.P., Hembeck, L., Vinciguerra, T.P., Anderson, D.C., Goldberg, D.L., Carpenter, S.F., Allen, D.J., Loughner, C.P., Salawitch, R.J., Dickerson, R.R., 2015. Ozone and NO_x chemistry in the eastern US: evaluation of CMAQ/CB05 with satellite (OMI) data. *Atmos. Chem. Phys.* 15 (19), 10965–10982. <http://dx.doi.org/10.5194/acp-15-10965-2015>.
- Chen, D., Zhao, Y., Nelson, P., Li, Y., Wang, X., Zhou, Y., Lang, J., Guo, X., 2016. Estimating ship emissions based on AIS data for port of Tianjin, China. *Atmos. Environ.* 145, 10–18. <http://dx.doi.org/10.1016/j.atmosenv.2016.08.086>.
- Chen, D., Wang, X., Li, Y., Lang, J., Zhou, Y., Guo, X., Zhao, Y., 2017a. High-spatio-temporal-resolution ship emission inventory of China based on AIS data in 2014. *Sci. Total Environ.* 609, 776–787. <http://dx.doi.org/10.1016/j.scitotenv.2017.07.051>.
- Chen, D., Zhao, N., Lang, J., Zhou, Y., Wang, X., Li, Y., Zhao, Y., Guo, X., 2017b. Contribution of ship emissions to the concentration of PM_{2.5}: a comprehensive study using AIS data and WRF/Chem model in Bohai Rim Region, China. *Sci. Total Environ.* 610–611, 1476–1486. <http://dx.doi.org/10.1016/j.scitotenv.2017.07.255>.
- Cleary, P.A., et al., 2015. Ozone distributions over southern Lake Michigan: comparisons between ferry-based observations, shoreline-based DOAS observations and model forecasts. *Atmos. Chem. Phys.* 15 (9), 5109–5122. <http://dx.doi.org/10.5194/acp-15-5109-2015>.
- CMAS, 2014. SMOKE v3.6 User's Manual. Edited. The Institute for the Environment, University of North Carolina, Chapel Hill.
- Cohan, D.S., Chen, R., 2014. Modeled and observed fine particulate matter reductions from state attainment demonstrations. *J. Air Waste Manag. Assoc.* 64 (9), 995–1002. <http://dx.doi.org/10.1080/10962247.2014.905509>.
- Cohen, A.J., et al., 2005. The global burden of disease due to outdoor air pollution. *J. Toxicol. Environ. Health A* 68 (13–14), 1301–1307. <http://dx.doi.org/10.1080/15287390590936166>.
- Cooper, D.A., 2003. Exhaust emissions from ships at berth. *Atmos. Environ.* 37 (27), 3817–3830. [http://dx.doi.org/10.1016/S1352-2310\(03\)00446-1](http://dx.doi.org/10.1016/S1352-2310(03)00446-1).
- Corbett, J.J., Koehler, H.W., 2003. Updated emissions from ocean shipping. *J. Geophys. Res. Atmos.* 108 (D20) doi:Artn 4650 10. 1029/2003jd003751.
- Corbett, J.J., Winebrake, J.J., Green, E.H., Kasibhatla, P., Eyring, V., Lauer, A., 2007. Mortality from ship emissions: a global assessment. *Environ. Sci. Technol.* 41 (24), 8512–8518. <http://dx.doi.org/10.1021/es071686z>.
- Digar, A., Cohan, D.S., Cox, D.D., Kim, B.U., Boylan, J.W., 2011. Likelihood of achieving air quality targets under model uncertainties. *Environ. Sci. Technol.* 45 (1), 189–196. <http://dx.doi.org/10.1021/es102581e>.
- Duncan, B.N., et al., 2010. Application of OMI observations to a space-based indicator of NO_x and VOC controls on surface ozone formation. *Atmos. Environ.* 44 (18), 2213–2223. <http://dx.doi.org/10.1016/j.atmosenv.2010.03.010>.
- EPA, 1970. The clean air act. 42 U.S.C. §7401 seq.
- EPA, 1990. Clean air act amendments of 1990. Public law. 549.
- EPA, 2002. Commercial marine emissions inventory development. EPA420-R-02-019.
- EPA, 2008. Act to prevent pollution from ships to implement MARPOL Annex VI. In: Congress (Ed.), Public Law 110-280, pp. 6.
- EPA, 2009a. Current Methodologies in Preparing Mobile Source Port Related Emissions Inventories. Final Report. <http://archive.epa.gov/sectors/web/pdf/ports-emission-inv-april09.pdf>.
- EPA, 2009b. Regulatory impact analysis: control of emissions of air pollution from category 3 marine diesel engines. EPA-420-R-09-019.
- EPA, 2010. Primary National Ambient Air Quality Standards for Nitrogen Dioxide; Final Rule, vol 75. pp. 6474–6537.
- EPA, 2014. In: OAQPS (Ed.), Meteorological Model Performance for Annual 2011 WRF v3.4 Simulation.
- EPA, 2015a. 2011 National Emissions Inventory, Version 2 Technical Support Document. https://www.epa.gov/sites/production/files/2015-2010/documents/nei2011v2012_

- tsd_2014aug2015.pdf.
- EPA, 2015b. 2014 NEI Commercial Marine Vessels - Final. https://www.epa.gov/sites/production/files/2015-2012/documents/2014_nei_commercial_marine_vessels_reviewdraft20151217_cleaned.pdf.
- EPA, 2015c. National Ambient Air Quality Standards for ozone; final rule. Fed. Reg. 80, 65293–65467.
- EPA, 2016. Multi-pollutant Comparison, Edited. United States Environmental Protection Agency. <https://www.epa.gov/air-emissions-inventories/multi-pollutant-comparison>.
- ERG, 2010. Documentation for the Commercial Marine Vessel Component of the National Emissions Inventory Methodology. Eastern Research Group (ERG) No. 0245.02.302.001; Contract No. EP-D-07-097.
- Eyring, V., Kohler, H.W., van Aardenne, J., Lauer, A., 2005. Emissions from international shipping: 1. The last 50 years. *J. Geophys. Res. Atmos.* 110 (D17) doi:Artn D17305 10.1029/2004jd005619.
- Eyth, A., Driver, L. (EPA), Personal e-mail communication, September 21, 2017.
- Gégo, E., Porter, P.S., Gilliland, A., Rao, S.T., 2007. Observation-based assessment of the impact of nitrogen oxides emissions reductions on ozone air quality over the eastern United States. *J. Appl. Meteorol. Climatol.* 46 (7), 994–1008. <http://dx.doi.org/10.1175/jam2523.1>.
- Goldberg, D.L., Loughner, C.P., Tzortziou, M., Stehr, J.W., Pickering, K.E., Marufu, L.T., Dickerson, R.R., 2014. Higher surface ozone concentrations over the Chesapeake Bay than over the adjacent land: observations and models from the DISCOVER-AQ and CBODAQ campaigns. *Atmos. Environ.* 84, 9–19. <http://dx.doi.org/10.1016/j.atmosenv.2013.11.008>.
- Goldberg, D.L., et al., 2016. CAMx ozone source attribution in the eastern United States using guidance from observations during DISCOVER-AQ Maryland. *Geophys. Res. Lett.* 43 (5), 2249–2258. <http://dx.doi.org/10.1002/2015gl067332>.
- González Abad, G., Liu, X., Chance, K., Wang, H., Kurosu, T.P., Suleiman, R., 2015. Updated smithsonian astrophysical observatory ozone monitoring instrument (SAO OMI) formaldehyde retrieval. *Atmos. Meas. Tech.* 8 (1), 19–32. <http://dx.doi.org/10.5194/amt-8-19-2015>.
- He, H., Hembeck, L., Hosley, K.M., Canty, T.P., Salawitch, R.J., Dickerson, R.R., 2013. High ozone concentrations on hot days: the role of electric power demand and NO_x emissions. *Geophys. Res. Lett.* 40 (19), 5291–5294. <http://dx.doi.org/10.1002/grl.50967>.
- IMO, 2014. Implications of the united nations convention on the law of the sea for the international maritime organization. LEG/MISC 8.
- Jacob, D.J., 2000. Heterogeneous chemistry and tropospheric ozone. *Atmos. Environ.* 34 (12–14), 2131–2159. [http://dx.doi.org/10.1016/S1352-2310\(99\)00462-8](http://dx.doi.org/10.1016/S1352-2310(99)00462-8).
- Kleinman, L.I., 1994. Low and high NO_x tropospheric photochemistry. *J. Geophys. Res. Atmos.* 99 (D8), 16831–16838. <http://dx.doi.org/10.1029/94jd01028>.
- Kleinman, L.I., Daum, P.H., Imre, D.G., Lee, J.H., Lee, Y.N., Nunnermacker, L.J., Springston, S.R., Weinstein-Lloyd, J., Newman, L., 2000. Ozone production in the New York City urban plume. *J. Geophys. Res. Atmos.* 105 (D11), 14495–14511. <http://dx.doi.org/10.1029/2000jd900011>.
- Kleinman, L.I., Daum, P.H., Lee, Y.N., Nunnermacker, L.J., Springston, S.R., Weinstein-Lloyd, J., Rudolph, J., 2001. Sensitivity of ozone production rate to ozone precursors. *Geophys. Res. Lett.* 28 (15), 2903–2906. <http://dx.doi.org/10.1029/2000gl012597>.
- Kleinman, L.I., 2005. The dependence of tropospheric ozone production rate on ozone precursors. *Atmos. Environ.* 39 (3), 575–586. <http://dx.doi.org/10.1016/j.atmosenv.2004.08.047>.
- Krotkov, N.A., Veefkind, P., 2016. OMI/Aura Nitrogen Dioxide (NO₂) Total and Tropospheric Column 1-orbit L2 Swath 13x24 km V003 Greenbelt. Goddard Earth Sciences Data and Information Services Center (GES DISC), MD, USA. <http://dx.doi.org/10.5067/Aura/OMI/DATA2017>. Accessed date: April 2017.
- Krotkov, N.A., Lamsal, L.N., Celarier, E.A., Swartz, W.H., Marchenko, S.V., Bucsela, E.J., Chan, K.L., Wenig, M., 2017. The version 3 OMI NO₂ standard product. *Atmos. Meas. Tech. Discuss.* 2017, 1–42. <http://dx.doi.org/10.5194/amt-2017-44>.
- Lamsal, L.N., Martin, R.V., Padmanabhan, A., van Donkelaar, A., Zhang, Q., Sioris, C.E., Chance, K., Kurosu, T.P., Newchurch, M.J., 2011. Application of satellite observations for timely updates to global anthropogenic NO_x emission inventories. *Geophys. Res. Lett.* 38 (5) n/a-n/a, doi:Artn L05810 10.1029/2010gl046476.
- Lawrence, M.G., Crutzen, P.J., 1999. Influence of NO_x emissions from ships on tropospheric photochemistry and climate. *Nature* 402 (6758), 167–170. <http://dx.doi.org/10.1038/46013>.
- Levelt, P.F., Hilsenrath, E., Leppelmeier, G.W., van den Oord, G.H.J., Bhartia, P.K., Tamminen, J., de Haan, J.F., Veefkind, J.P., 2006a. Science objectives of the ozone monitoring instrument. *IEEE Trans. Geosci. Remote Sens.* 44 (5), 1199–1208. <http://dx.doi.org/10.1109/Tgrs.2006.872336>.
- Levelt, P.F., van den Oord, G.H.J., Dobber, M.R., Malkki, A., Huib, V., Johan de, V., Stammes, P., Lundell, J.O.V., Saari, H., 2006b. The ozone monitoring instrument. *IEEE Trans. Geosci. Remote Sens.* 44 (5), 1093–1101. <http://dx.doi.org/10.1109/Tgrs.2006.872333>.
- Liao, K.J., Hou, X.T., Baker, D.R., 2014. Impacts of interstate transport of pollutants on high ozone events over the Mid-Atlantic United States. *Atmos. Environ.* 84, 100–112. <http://dx.doi.org/10.1016/j.atmosenv.2013.10.062>.
- Loughner, C.P., Allen, D.J., Pickering, K.E., Zhang, D.L., Shou, Y.X., Dickerson, R.R., 2011. Impact of fair-weather cumulus clouds and the Chesapeake Bay breeze on pollutant transport and transformation. *Atmos. Environ.* 45 (24), 4060–4072. <http://dx.doi.org/10.1016/j.atmosenv.2011.04.003>.
- Loughner, C.P., et al., 2014. Impact of Bay-breeze circulations on surface air quality and boundary layer export. *J. Appl. Meteorol. Climatol.* 53 (7), 1697–1713. <http://dx.doi.org/10.1175/Jamc-D-13-0323.1>.
- Madronich, S., 2014. Atmospheric chemistry: ethanol and ozone. *Nat. Geosci.* 7 (6), 395–397. <http://dx.doi.org/10.1038/ngeo2168>.
- Marvin, M.R., et al., 2017. Impact of evolving isoprene mechanisms on simulated formaldehyde: an inter-comparison supported by in situ observations from SENEX. *Atmos. Environ.* 164, 325–336. <http://dx.doi.org/10.1016/j.atmosenv.2017.05.049>.
- Mazzuca, G.M., Ren, X.R., Loughner, C.P., Estes, M., Crawford, J.H., Pickering, K.E., Weinheimer, A.J., Dickerson, R.R., 2016. Ozone production and its sensitivity to NO_x and VOCs: results from the DISCOVER-AQ field experiment, Houston 2013. *Atmos. Chem. Phys.* 16 (22), 14463–14474. <http://dx.doi.org/10.5194/acp-16-14463-2016>.
- McDill, J., McCusker, S., Sabo, E., 2015. Technical Support Document: Emission Inventory Development for 2011, 2018, and 2028 for the Northeastern US Alpha 2 Version. http://www.marama.org/images/stories/documents/2011-2018-2028_Technical_Support_Docs/TSD_ALPHA2_Northeast_Emission_Inventory_for_2011_2018_2028_DraftFinal_20151123.pdf.
- Millet, D.B., et al., 2006. Formaldehyde distribution over North America: implications for satellite retrievals of formaldehyde columns and isoprene emission. *J. Geophys. Res. Atmos.* 111 (D24) doi:Artn D24s02 10.1029/2005jd006853.
- Murphy, S.M., et al., 2009. Comprehensive simultaneous shipboard and airborne characterization of exhaust from a modern container ship at sea. *Environ. Sci. Technol.* 43 (13), 4626–4640. <http://dx.doi.org/10.1021/es802413j>.
- Otte, T.L., Pleim, J.E., 2010. The Meteorology-Chemistry Interface Processor (MCIP) for the CMAQ modeling system: updates through MCIPv3.4.1. *Geosci. Model Dev.* 3 (1), 243–256.
- Pirjola, L., Pajunaja, A., Walden, J., Jalkanen, J.P., Ronkko, T., Kousa, A., Koskentalo, T., 2014. Mobile measurements of ship emissions in two harbour areas in Finland. *Atmos. Meas. Tech.* 7 (1), 149–161. <http://dx.doi.org/10.5194/amt-7-149-2014>.
- Pope 3rd, C.A., Burnett, R.T., Thun, M.J., Calle, E.E., Krewski, D., Ito, K., Thurston, G.D., 2002. Lung cancer, cardiopulmonary mortality, and long-term exposure to fine particulate air pollution. *JAMA* 287 (9), 1132–1141. <http://dx.doi.org/10.1001/jama.287.9.1132>.
- Ruiz, L.H., Yarwood, G., 2013. Interactions between Organic Aerosol and NO_x: Influence on Oxidant Production. Texas Air Quality Research Program Project 12-012, University of Texas, Austin, TX and ENVIRON International Corporation, Novato, CA.
- Sillman, S., 1999. The relation between ozone, NO_x and hydrocarbons in urban and polluted rural environments. *Atmos. Environ.* 33 (12), 1821–1845. [http://dx.doi.org/10.1016/S1352-2310\(98\)00345-8](http://dx.doi.org/10.1016/S1352-2310(98)00345-8).
- Sillman, S., 2002. Some theoretical results concerning O₃-NO_x-VOC chemistry and NO_x-VOC indicators. *J. Geophys. Res.* 107 (D22). <http://dx.doi.org/10.1029/2001jd001123>.
- Skamarock, W.C., Klemp, J.B., Dudhia, J., Gill, D.O., Barker, D.M., Duda, M.G., Huang, X.-Y., Wang, W., Powers, J.G., 2008. A description of the advanced research WRF version 3. NCAR Tech. Note NCAR/TN-475+STR 119. <http://dx.doi.org/10.5065/D68S4MVH>.
- Sorooshian, A., Prabhakar, G., Jonsson, H., Woods, R.K., Flagan, R.C., Seinfeld, J.H., 2015. On the presence of giant particles downwind of ships in the marine boundary layer. *Geophys. Res. Lett.* 42 (6), 2024–2030. <http://dx.doi.org/10.1002/2015gl063179>.
- Stauffer, R.M., Thompson, A.M., Martins, D.K., Clark, R.D., Goldberg, D.L., Loughner, C.P., Delgado, R., Dickerson, R.R., Stehr, J.W., Tzortziou, M.A., 2015. Bay breeze influence on surface ozone at Edgewood, MD during July 2011. *J. Atmos. Chem.* 72 (3–4), 335–353. <http://dx.doi.org/10.1007/s10874-012-9241-6>.
- Trail, M., Tsimpidi, A.P., Liu, P., Tsigaridis, K., Rudokas, J., Miller, P., Nenes, A., Hu, Y., Russell, A.G., 2014. Sensitivity of air quality to potential future climate change and emissions in the United States and major cities. *Atmos. Environ.* 94, 552–563. <http://dx.doi.org/10.1016/j.atmosenv.2014.05.079>.
- Travis, K.R., et al., 2016. Why do models overestimate surface ozone in the Southeast United States? *Atmos. Chem. Phys.* 16 (21), 13561–13577. <http://dx.doi.org/10.5194/acp-16-13561-2016>.
- UN, 2015. Review of Maritime Transport, Paper Presented at United Nations Conference on Trade and Development. United Nations, New York and Geneva.
- Vinciguerra, T., Bull, E., Canty, T., He, H., Zalewsky, E., Woodman, M., Aburn, G., Ehrman, S., Dickerson, R.R., 2017. Expected ozone benefits of reducing nitrogen oxide (NO_x) emissions from coal-fired electricity generating units in the eastern United States. *J. Air Waste Manag. Assoc.* 67 (3), 279–291. <http://dx.doi.org/10.1080/10962247.2016.1230564>.
- Vinken, G.C.M., Boersma, K.F., van Donkelaar, A., Zhang, L., 2014. Constraints on ship NO_x emissions in Europe using GEOS-Chem and OMI satellite NO₂ observations. *Atmos. Chem. Phys.* 14 (3), 1353–1369. <http://dx.doi.org/10.5194/acp-14-1353-2014>.
- Wayland, R., 2014. Draft Modeling Guidance for Demonstrating Attainment of Air Quality Goals for Ozone, PM_{2.5}, and Regional Haze. http://www3.epa.gov/scram001/guidance/guide/Draft_O3-PM-RH_Modeling_Guidance-2014.pdf.
- Williams, E.J., Lerner, B.M., Murphy, P.C., Herndon, S.C., Zahniser, M.S., 2009. Emissions of NO_x, SO₂, CO, and HCHO from commercial marine shipping during Texas Air Quality Study (TexAQSt) 2006. *J. Geophys. Res. Atmos.* 114 (D21) doi:Artn D21306 10.1029/2009jd012094.
- Yarwood, G.S., Rao, S., Yocke, M., Whitten, G.Z., 2005. Updates to the Carbon Bond Chemical Mechanism: CB05. http://www.camx.com/publ/pdfs/CB05_Final_Report_120805.pdf.
- Yarwood, G.S., Whitten, G.Z., Jung, J., Heo, G., Allen, D., 2010. Development, Evaluation and Testing of Version 6 of the Carbon Bond Chemical Mechanism (CB6). <https://www.tceq.texas.gov/assets/public/implementation/air/am/contracts/reports/pm/5820784005FY1026-20100922-environ-cb6.pdf>.
- Yu, S., Mathur, R., Kang, D., Schere, K., Eder, B., Pleim, J., 2006. Performance and diagnostic evaluation of ozone predictions by the eta-Community Multiscale Air Quality forecast system during the 2002 New England Air Quality Study. *J. Air Waste Manag. Assoc.* 56 (10), 1459–1471. <http://dx.doi.org/10.1080/10473289.2006.10464554>.